Available online at www.sciencedirect.com
SCIENCE DIRECT
Journal of Nuclear Materials 349 (2006) 251–264
journal of nuclear materials
www.elsevier.com/locate/jnucmat

# Characteristics of microscopic strain localization in irradiated 316 stainless steels and pure vanadium

T.S. Byun *, N. Hashimoto, K. Farrell, E.H. Lee

*Oak Ridge National Laboratory, P.O. Box 2008, MS-6151, Oak Ridge, TN 37831, USA*

Received 1 August 2005; accepted 31 October 2005

**Abstract**

Characteristics of localized dislocation glide were investigated for 316 and 316LN stainless steels and pure vanadium after ion or neutron irradiation near room temperature and deformation by a uniaxial tensile load or by a multiaxial bending load. In the irradiated 316 stainless steels, both the uniaxial tensile loading and the multiaxial bend loading produced straight localized bands in the form of channels and twins. In vanadium specimens, on the other hand, curved channels were observed after tensile deformation, and these became a common feature after multiaxial bend deformation. No twin was observed in vanadium. A river pattern of channels was observed in the bent samples after irradiation to a high dose of 0.69 dpa. A highly curved channel can be formed by successive cross slip of screw dislocations. Also, the channel width was not constant along the channels; channel widening occurred when weak defect clusters were removed by the gliding screw dislocations changing their paths by cross slip. It is believed that the dissociation of dislocations into partials and high angles between easy glide planes suppresses the formation of curved channels, while a multiaxial stress state, or a higher stress constraint, increases the tendency for channel bending and widening.


## 1. Introduction

Irradiation with energetic particles hardens a metallic material by producing numerous small defect clusters and makes it more prone to localized dislocation glide during plastic deformation [1–3]. The microscopic mechanisms of strain localization often observed in irradiated materials are dislocation channeling [1–16] and deformation twinning [15–23]. A number of studies have detailed the features for these mechanisms [1–26]. It was shown that in low stacking fault energy materials deformation twinning is an alternative localization mechanism to channeling and that the two mechanisms have many similarities [15,16,23]. However, those strain localization behaviors have not been fully characterized as functions of material properties and testing conditions.

As known for decades, dislocation channeling is a process of heterogeneous plastic deformation by ordinary dislocations, in which dislocations released from a source glide along the limited slip planes within the band, removing or cutting through small barriers in their paths [1–11]. This defect-clearing interaction creates an easy path for subsequent dislocation glide and a narrow channel a fraction of a

* Corresponding author. Tel.: +1 865 576 7738; fax: +1 865 574 0641.
*E-mail address:* byunts@ornl.gov (T.S. Byun).

0022-3115/$ - see front matter © 2005 Elsevier B.V. All rights reserved.
doi:10.1016/j.jnucmat.2005.10.011

micron wide is developed. It has been observed that the strain in a channel reaches a few hundred percent, even at a bulk strain of a few percent [6,7,15]. On the other hand, the deformation twinning, also called mechanical twinning, is a localized deformation mechanism by partial dislocations [24–26]. In face-centered cubic (fcc) alloys with low stacking fault energy (SFE), the deformation twins are formed by glide of Shockley partial dislocations of the same sign on successive {1 1 1} planes [18–27]. In such a twin shear strain is 70.7% [24] and the number density of defects is reduced by glide of partial dislocations [18,19].

In previous papers on strain localization mechanisms [15,18–20,23], the twinning mechanism was treated in a similar manner to channeling, except for the existence of stacking faults. Both mechanisms produce well-defined deformation paths led by the first gliding dislocation, or probably by the first group of gliding dislocations in the band, which reduce resistance to subsequent glides. A common condition for the two mechanisms is high stress, which suggests that any strengthening mechanism can promote the tendency for strain localization [28]. Although the two different mechanisms share common features, differences in the details of material and test conditions produce a variety of strain localization features. First, the SFE must be an intrinsic material property that plays an important role in every process of plastic deformation. Straight, well-confined channels and twins are formed in low SFE materials because large separation of partial dislocations due to the low SFE prohibits cross slip, which is needed in order to change glide plane [29,30]. The most significant difference in deformation characteristics due to different SFE might be the types of dislocations responsible for the mechanisms; channeling is formed by glide of ordinary dislocations, while twinning involves partial dislocations [23]. Second, the characteristics of defect clusters or precipitate particles may change the deformation behavior. For example, wide and clear channels may develop if the defect clusters in an irradiated material are weak, and therefore they can be easily removed by interactions with gliding dislocations [1–3]. Third, the testing conditions, such as stress state, strain rate, and temperature, may affect the mechanism and shape of strain localization. A high strain rate can promote strain localization because a high stress level, which may be critical for the localization mechanisms, can be achieved [15,23]. Further, the stress state, or constraint of deformation, may affect the shape and size distributions of localized bands because a complex stress field in highly constrained deformation will activate more sources and slip systems, and raises the need for cross slip to produce a deformation compatible with the stress field [31].

In the past few years microscopic strain localization has been observed by the authors in many metallic materials after low temperature irradiation [11–15,18–23]. In this study, two extreme cases, 316 stainless steel (fcc) and pure vanadium (bcc; body-centered cubic), were selected for a comparative study focusing on the shape of the strain localization bands. The former material represents a low SFE ($<20\ mJ/m^2$) material showing straight, fine localization bands, while the latter material is a high SFE material and it produces complex channeling features.

## 2. Experimental

### 2.1. Materials and specimens

Test materials were two variants of 316 stainless steel: a conventional 316 stainless steel (Fe–13.45Ni–17.15Cr–2.34Mo–0.059C–1.86Mn–0.57Si–0.018S–0.024P–0.1Cu–0.02Co–0.031N, in wt%) and a 316LN stainless steel (Fe–10.2Ni–16.3Cr–2.01Mo–1.75Mn–0.39Si–0.11N–0.029P), and a 99.8wt% pure vanadium (V–0.026Si–0.039Mo–0.027O–0.0096N–0.0024C). 0.25 mm thick tensile specimens and 3 mm diameter TEM disks were vacuum-annealed before irradiation; the stainless steel specimens were annealed at 1050 °C for 30 min and the vanadium specimens at 900 °C for 30 min. Average grain sizes were about 65 and 30 μm for 316 stainless steel and vanadium, respectively. The grain size for 316LN steel was not measured. No preferred grain orientation was observed in all test materials. The gage sections of the tensile specimens were 2 or 1.5 mm wide and 7.6 or 8 mm long (for ion irradiation and neutron irradiation, respectively). Square TEM specimens were taken from irradiated and deformed tensile specimens. Regular size TEM disks, 3mm in diameter and 0.25 mm in thickness, were used for disk bend deformation to apply a biaxial stress.

Neutron irradiation was performed in the Hydraulic Tube (HT) facility of the High Flux Isotope Reactor (HFIR) at the Oak Ridge National Laboratory (ORNL). Irradiation doses achieved from the HFIR HT facility were 0.0001–0.69 dpa

Table 1
Irradiation and deformation conditions for sheet tensile and disk specimens

| Case no. | Material | Irradiation condition | Dose [dpa] | Load | Equivalent strain [%] |
|---|---|---|---|---|---|
| 1 | 316LN (FCC) | 350 keV $He^+$, 200 °C | 0–3.7 | Tensile | 16–20 |
| 2 | 316LN (FCC) | 350 keV $He^+$, 200 °C | 0–1.5 | Disk bend | 10 |
| 3 | 316 (FCC) | Fast neutron, 60–100 °C | 0.78 | Tensile | 32 |
| 4 | V (99.8% purity, BCC) | Fast neutron, 60–100 °C | 0–0.12 | Tensile | 0.1–0.3 |
| 5 | V (99.8% purity, BCC) | Fast neutron, 60–100 °C | 0.69 | Disk bend | 5–12 |

for pure vanadium and 0.0001–0.78 dpa for 316 stainless steel [11]. In this HFIR irradiation the fluence to dpa ratios were about $1.1 \times 10^{25}$ and $9.2 \times 10^{24}$ n $m^{-2}$/dpa ($E > 0.1$ MPa) for 316 stainless steel and vanadium, respectively. Irradiation temperatures were in the range 60–100 °C. Irradiation with helium ions was performed at the Triple Ion Facility at ORNL. The polished sides of the plate tensile specimens and the 3 mm disks were irradiated up to 15 dpa (or 20 at.% He) at 200 °C with 360 keV He ions using a 2.5 MV Van de Graaff accelerator. Maximum helium deposition and displacement damage occurred at a depth of 700–800 nm [32,33]. Details of these irradiation experiments have been published [18–20].

Tensile specimens were deformed in screw-driven tensile machines at a nominal strain rate of about $10^{-3}$ $s^{-1}$, while TEM disks were deformed using a ball indentation technique at a similar strain rate, which provides multiaxial loading conditions [20–22]. Preparation and deformation procedures for the ion irradiated specimens were specially designed. The polished-and-irradiated side of the disk was placed face down onto the circular recess of a die with edge clamping, and a load was applied to the top of the disk through a tungsten carbide (WC) ball of 1 mm diameter via a rod plunger of 1 mm diameter. After deformation the surface layer to a depth of about 600 nm was removed from the specimen by electrochemical polishing. The new surface was marked with a protective lacquer before twin-jet polishing to produce thin film area for TEM observation. This method revealed deformation microstructures in the highest damage region. The surface removal operation was omitted in the neutron-irradiated disks where radiation damage is uniform throughout each specimen, and the stress level was estimated for the middle thickness region of the disk. In the disk bend method, strain was calculated from the thickness change by deformation, and stress was obtained from the corresponding tensile test curve at the same strain [21,22]. A detailed description for the disk bend method has been published [21]. Table 1 summarizes experiment conditions for each case. A Philips CM12 electron microscope was used at 120 keV operating voltage for examination of the deformation microstructures.

## 3. Results

### 3.1. Twins and channels in austenitic stainless steels

In irradiated austenitic stainless steels both twinning and channeling mechanisms are operative depending on the type of defect clusters and on the testing condition [15,22,23]. Channels have been observed primarily in neutron irradiated specimens, where the material was hardened by removable, nanometer size defect clusters [1–14]. However, twins were dominant in the helium-irradiated specimens, which were hardened by helium gas bubbles as well as by displacement damage [15–23]. The helium bubbles can be sheared, but cannot be removed by dislocations [18–20,23]. The sheared bubbles with ledges may be harder obstacles than the original spherical bubbles and they might continue to be effective as barriers to dislocation glide [19,23]. Twinning is preferred in this high stress condition because its initiation requires higher local stress within the band [15,23].

Fig. 1(a)–(c) present the microstructures in unirradiated or helium irradiated 316LN stainless steel after uniaxial tensile deformation. Fig. 1(a) shows typical tangled dislocations formed in an unirradiated specimen with a preferred alignment along (1 1 1) slip planes. In Fig. 1(b), the dissociated dislocations in the low SFE alloy often form stacking faults and microtwins in a more localized manner than the background tangled dislocations [22–24,29]. At 3.7 dpa the alloy was deformed only by mechanical twinning, as seen in Fig. 1(c). It is known that at room temperature twinning, which occurs above a critical stress of about 600 MPa [23], is the only possible mechanism in the specimens

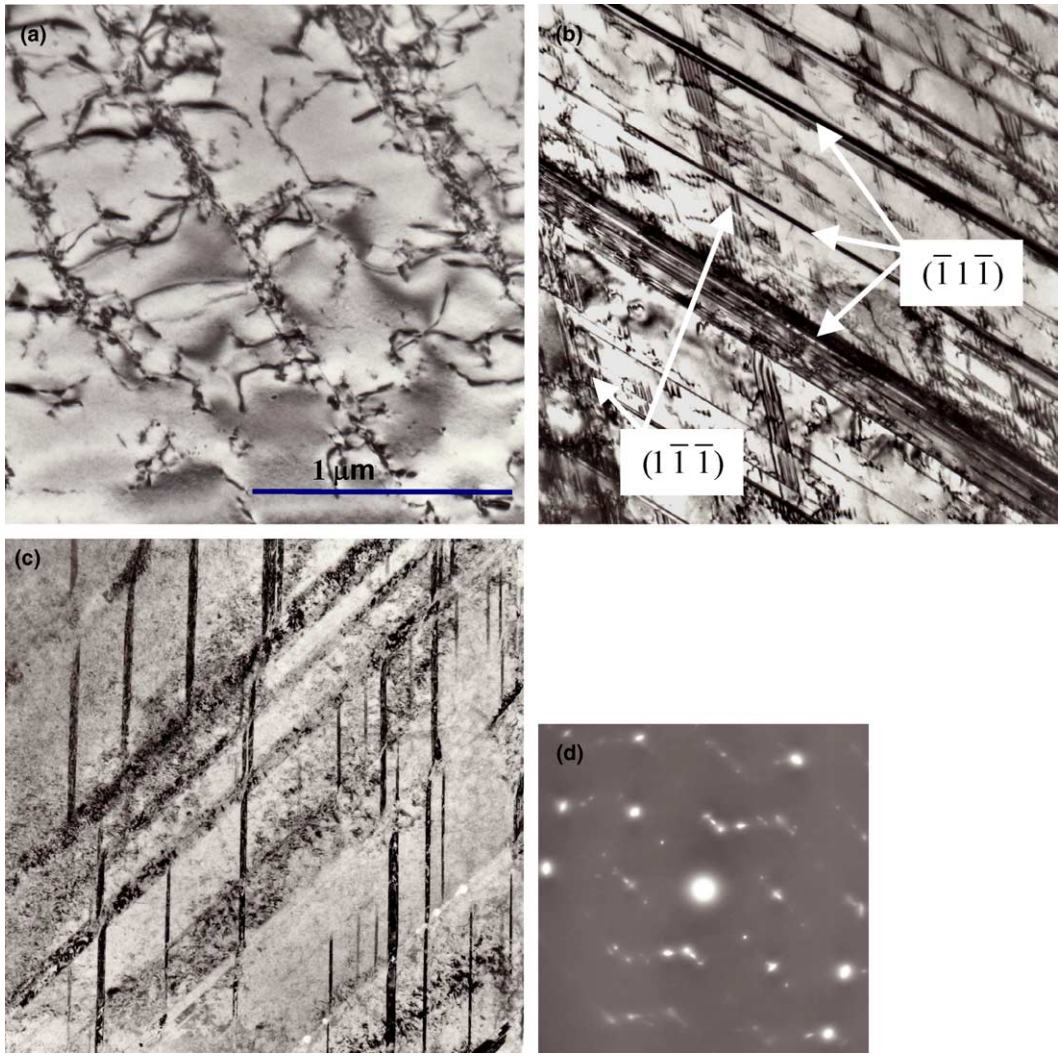


Fig. 1. Deformation microstructures of 316LN stainless steel after tensile deformation: (a) dislocation tangles at 16% strain before irradiation, (b) twins and tangles at 20% strain before irradiation, (c) twins after irradiating to 3.7 dpa with helium ions, followed by tensile straining to 20%, and (d) diffraction pattern of (c) showing twin streaks. $\vec{Z}$(zone axis) $\approx$ [1 1 0] for (a)–(c). (Note that the zone axis of a crystal is a direction vector which belongs to a group of planes and coincides with the axis of incident electron beam. It is normal to the paper surface.) The distance marker in (a) is also valid for (b) and (c).

irradiated by helium ions to high doses because the non-removable helium bubbles continue to act as obstacles to dislocation glide [22]. In both Fig. 1(b) and (c), long twin bands are formed on a {1 1 1} plane and mostly segmented microtwins are formed intercepting the main twins, which are identified as thicker continuous bands and presumably formed before the segmented ones. No curved twin was found in the 316LN stainless steel. In the twin-dominant microstructures, the distance between twin bands is typically a fraction of a μm.

Bend loading generates a multiaxial, high constraint stress state within a disk specimen. Further, the ball indentation forms a bump in the central part of the disk specimen, which becomes a portion of spherical shell as the indentation progresses. Deformation with this curvature under multiaxial stress state should increase the possibility of cross slip in dislocation glide due to geometrical requirements. In the deformation microstructures of stainless steel, however, the effect of this complex stress state was not observed, as shown in Fig. 2(a)–(c). The tangled dislocations in Fig. 2(a) are not different from those in the tensile-deformed specimen. Straight bands are evident in Fig. 2(b), where the glide of partial dislocations is localized. Some

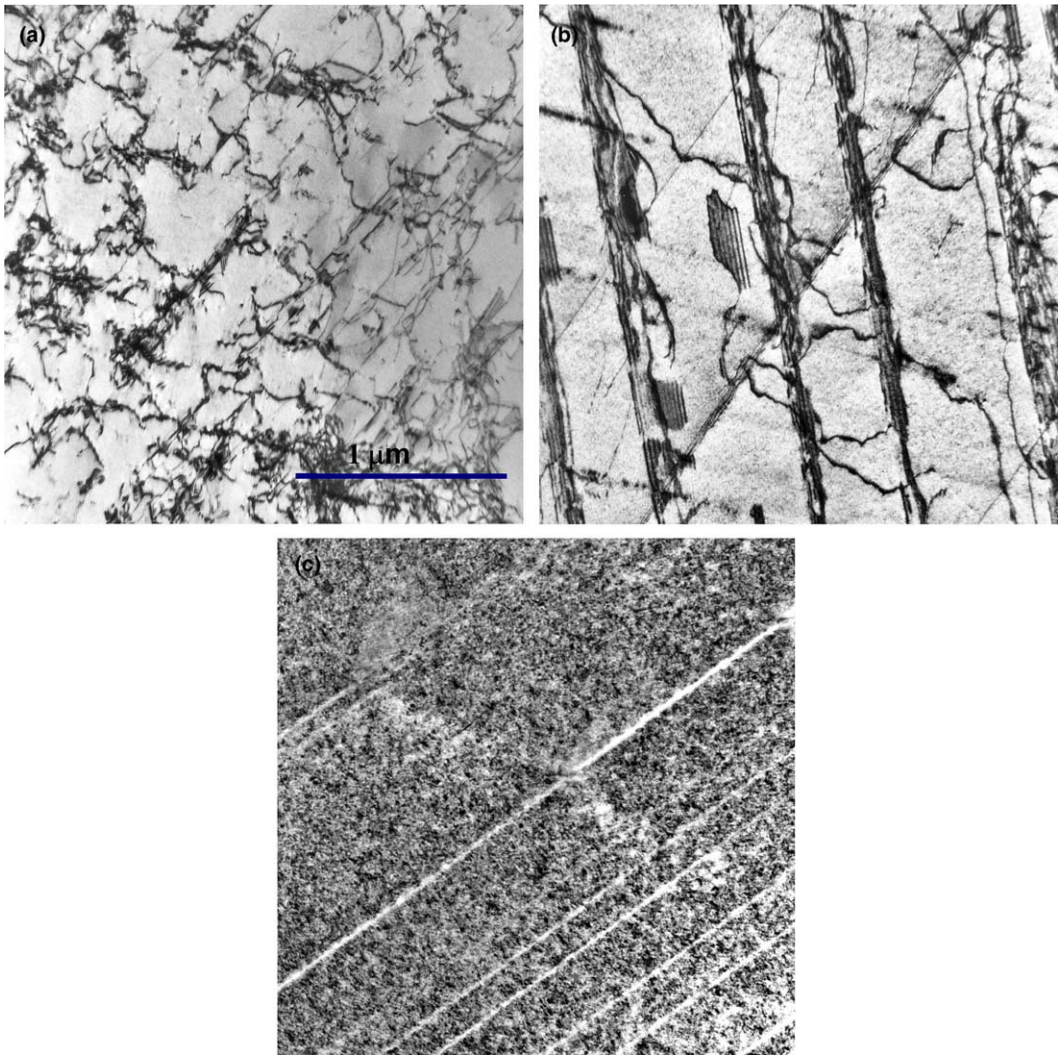


Fig. 2. Deformation microstructures of 316LN stainless steel after disk bend deformation to a strain of about 10%: (a) dislocation tangles in unirradiated specimen, (b) twins and stacking faults after irradiation to 0.15 dpa with helium ions, and (c) twins at 1.5 dpa. ($\vec{Z} \approx [110]$).

random dislocations and stacking faults are formed outside of twin and stacking fault bands. In Fig. 2(c) dislocation glide is completely restricted in the straight twin bands (white lines) formed on a single slip system.

As seen in Fig. 3, channeling is largely favored in the stainless steel specimen irradiated by neutrons at low temperature to a relatively high dose of 0.78 dpa [11]. The defect-cleared channels formed on $\{111\}$ planes intercept each other and divide the deformation microstructure into blocks with little dislocation activity in the surrounding matrix. It is known that the active $\{111\}\langle 110\rangle$ slip systems for channeling are the same as those with tangled dislocations [1–3,11]. With an average of 1–3 dislocations traveled on each slip plane in the channel [1–7], shear strain is well confined in the channel and is uniformly distributed through the width [6,7,11]. (Note that the total number of dislocations which have glided in a channel can be calculated by measuring an offset at an intersection with other channel or grain boundary and dividing the offset by the size of Burgers vector. Also, the number of planes in a channel can be calculated by measuring the width of the channel and dividing it by the inter-planner distance.) Although the secondary slip was active during the channel deformation, and therefore formed many crossings with the primary slip bands, no primary channel or secondary channel segment exhibited curvature in the low SFE fcc materials [6,7,14].

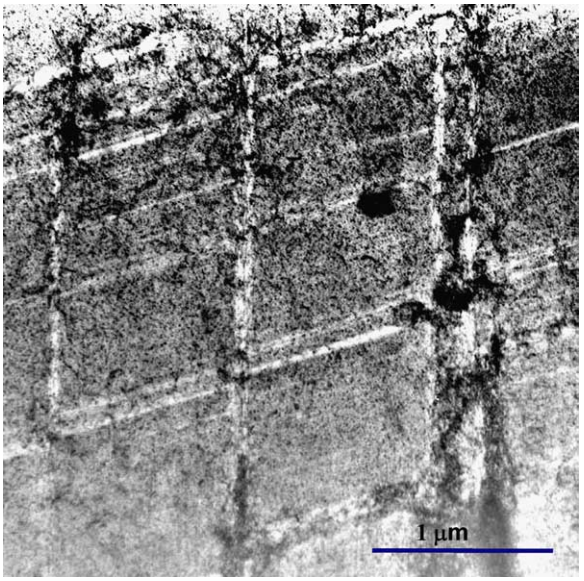


Fig. 3. Network of dislocation channels in 316 stainless steel irradiated by fast neutrons to 0.78 dpa and tensile strained 32%. ($\vec{Z} \approx [110]$).

### 3.2. Channels in pure vanadium

Fig. 4 presents the deformation microstructures of pure vanadium after tensile deformation [12]. Pure vanadium experiences strain localization by channeling only due to its high stacking fault energy that discourages twinning. Fig. 4(a)–(c) show a transition from dislocation tangle dominant to defect-cleared channel dominant microstructure as neutron dose increases. In unirradiated vanadium, random, tangled dislocations are dominant, Fig. 4(a). Plastic deformation is weakly channeled at 0.012 dpa, as seen in Fig. 4(b). Most of the remaining dislocations are confined within the band, whose boundary with the surrounding undeformed matrix is vague. In previous work [12] detailed deformation microstructures at this dose were characterized by a localized deformation band with elongated dislocations or a large dislocation pileup in it. It is believed that a dose of 0.012 dpa is about the critical dose for channeling in pure vanadium. The yield stress was 470 MPa for this 0.012 dpa case, which might be similar to the critical stress for channeling in pure vanadium. Most of the dislocations and pileups within the localized bands disappeared in the channels formed at a higher dose of 0.12 dpa [12]. Fig. 4(c) shows two straight channels intercepting each other and containing a small amount of black dot defects and dislocation segments. It is not clear if these are products of interactions between gliding dislocations and radiation-induced defect clusters, or unremoved defect clusters and extended grown-in dislocations formed during irradiation. A feature worth noting in Fig. 4(c) is that channel A is straight while channel B is offset at the intercept. This indicates that the channel B was formed first and then channel A was formed cutting through channel B. This can be taken as evidence that the two channels were formed at separate times. In this study no twinning was observed in irradiated vanadium [12,34].

Before discussing the microstructures of bent specimens, the amounts of strain applied are mentioned here for clarity in comparison. Since after low temperature irradiation to a dose of 0.01 dpa or higher the sheet tensile specimens experienced necking at a low plastic strain (<0.5%) and the necked section was too narrow to provide an observable TEM specimen, TEM samples were taken from the uniform deformation region only, where the bulk plastic strains were in the range of 0.1–0.3%, Fig. 4(b) and (c). In spite of these low bulk strains, the local plastic strains in the channeled areas were estimated to be several percent [15]. A higher bulk strain in the neck can be obtained by propagation of the channeled area or by formation of more channels within the area. This means that in channeled microstructures the deformation microstructure at low bulk strains may not be very different from those formed at higher bulk strains.

Fig. 5 presents a channel network in vanadium after neutron-irradiation to 0.69 dpa and disk bend deformation to 10% strain. This channel network is analogous to the river patterns of cleavage in bcc metals [24,29]; the channels can be splitting, merging, widening, and curving during propagation. Fig. 6(a)–(c) show the curved, widening dislocation channels at higher magnification. Fig. 6(a) shows two channels splitting, or merging; Fig. 6(b) shows a slightly curved channel with relatively constant width. An extreme case of a widening channel is seen in Fig. 6(c). In the widest part at the right side of the micrograph, the channel width is larger than 200 nm, which is about four times larger than that of the narrow side, about 50 nm. A few defects and dislocation segments are found inside the widened part of the channel. It is believed that the glide density, the number of dislocation glides per slip plane, in this area was less than that in the narrower part of the channel, and therefore radiation-induced defect clusters could not be completely

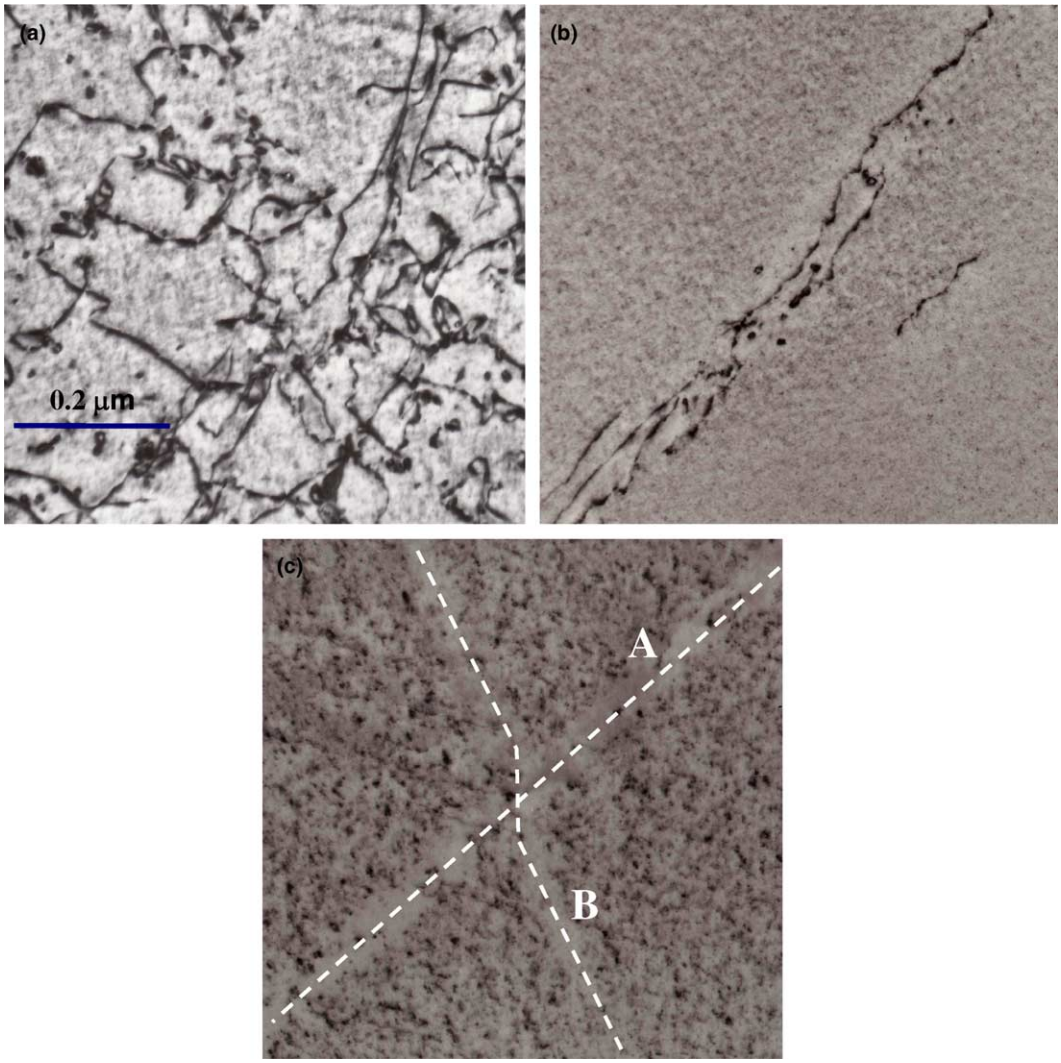


Fig. 4. Deformation microstructures in unirradiated and neutron-irradiated vanadium after tensile deformation ($\vec{Z} \approx [\bar{1}\,1\,1]$): (a) dislocation tangles at 10% strain at 0 dpa, (b) dislocations confined in a slip band after straining to 0.1% strain, at 0.012 dpa, (c) a channel intercepted by another after straining to 0.3%, at 0.12 dpa.

cleared. This is based on the assumption that the same number of dislocations have passed throughout the channel.

Only a perfect screw dislocation can change its slip plane by cross slip, in which its Burgers vector is not changed [24,29,30]. Since one cross slip onto another slip plane will make just a sharp deflection in the path of a dislocation, the curving and/or widening over a large area, as seen in Figs. 5 and 6, must be the culmination of accumulation of numerous cross slips. A curved path can be formed by multiple cross slips per each dislocation or by cross slips on successive planes at different positions with single cross slip per each dislocation. Part or all of the screw dislocations which glided through the channel have successively cross slipped as the channel advanced from the left to the right side.

Other important observation in Figs. 5 and 6 is the existence of dense grown-in dislocations formed by irradiation [34,35]. These were almost completely removed by the channeling process. Some dislocations observed within the channels are believed to be extended parts of grown-in dislocations from the non-channeled area. Also, the fact that channels do not include dense tangles indicates that the grown-in dislocations, along with black dot defect clusters, are removable obstacles to gliding dislocations.

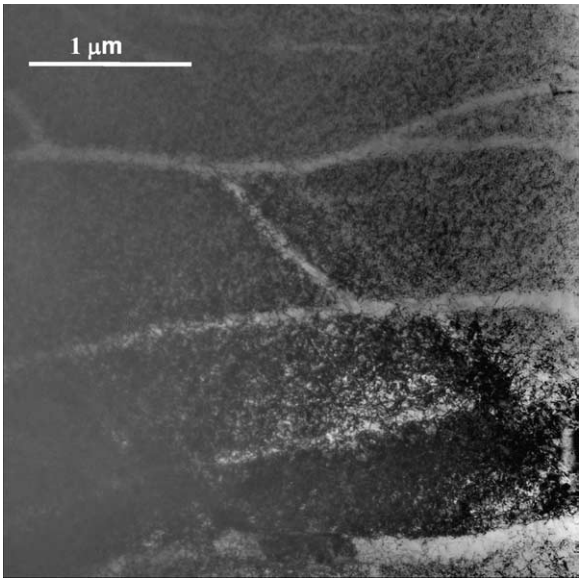


Fig. 5. Deformation microstructures in vanadium after neutron-irradiation to 0.69 dpa and disk bend deformation to 10% strain ($\vec{Z} \approx [\bar{1}\,1\,1]$).

## 4. Discussion

### 4.1. Stacking fault energy, crystal structure, and cross slip

As described in the preceding sections, significantly different features of strain localization are observed in austenitic stainless steels and pure vanadium. These differences may result from different material properties such as low stacking fault energy (SFE) vs. high SFE, fcc vs. bcc, and different strengths of radiation-induced defects. Also, the differences are probably exacerbated by external deformation conditions, such as stress state in loading and testing temperature.

The straight channels and twin bands in the stainless steels are believed to be caused by the low SFE of the steels ($<20$ mJ/m$^2$). In low SFE fcc materials, the ordinary dislocations with Burgers vector $\vec{b} = 1/2\langle 1\,1\,0\rangle$-type are dissociated into partial dislocations, $\vec{b}_p = 1/6\langle 1\,1\,2\rangle$-type, so-called leading and trailing partials [23,29,30]. In copper and austenitic stainless steels, the separation distance between the partial dislocations reaches only a few to a few tens of nanometers [23,36–38]. Once a perfect dislocation is dissociated into partials, a significantly higher stress is needed to recombine these into a perfect dislocation. This is because the stress fields of the partials include a repulsive stress component, and the interaction force is inversely proportional to the distance between the partials [30]. Further, in fcc metals gliding without dissociation should occur in a $\langle 1\,1\,0\rangle$ direction on a $\{1\,1\,1\}$ plane, and it is energetically unfavorable since atoms do not glide on the lowest energy valleys. This fact forces dislocations to be dissociated into partials to take the lowest energy valleys in the $\langle 1\,1\,2\rangle$ directions [29,30]. Although recombination of partials is difficult due to repulsive force between partials, the separation distance can be readily increased by application of an external stress. It has been shown that the separation distance can increase to infinity at an achievable stress level during tensile testing [15,22,23].

In polycrystalline materials a complex multiaxial stress field can be generated within a grain due to distortions by deformation and interactions between adjoining grains. Local material may deform by dislocation slip in a way to reduce the maximum amount of stress. The most effective way of reducing stresses will be the formation of slip bands following the maximum shear stress planes, which may have curvature. However, dislocation slip, which occurs on a limited number of slip systems, might be constrained by discrepancy between the maximum shear stress planes and the easy glide planes. Cross slip should occur to accommodate the complex stress and strain fields. Since cross slip can occur only by perfect screw dislocations, it may not occur if the gliding dislocations are dissociated. Therefore, any deformation bands in which cross slip is inhibited must be straight, as seen in Figs. 1 and 2, and more slip systems might operate to accommodate the complex stress field within a grain. Also, finer slip bands, Fig. 1(b), and segmentation of bands (twins), Fig. 1(c), are believed to be alternative ways of accommodating the complex stress field. Such deformation without cross slip should experience more interactions between the slip bands formed in different slip systems and therefore produces a higher strain-hardening rate. Further, relatively high internal stress might be generated in deformation without cross slip, since cross slip is not available to relax the constraint stress of deformation. Much of the internal stress will contribute to strain hardening in the form of long range back stress [29,39].

The easy glide plane in a crystalline material is usually the most closely packed plane [29]. In bcc crystals, atoms are closest in the $\langle 1\,1\,1\rangle$ directions and any plane containing one of these directions can be primary slip planes for dislocation glide. In

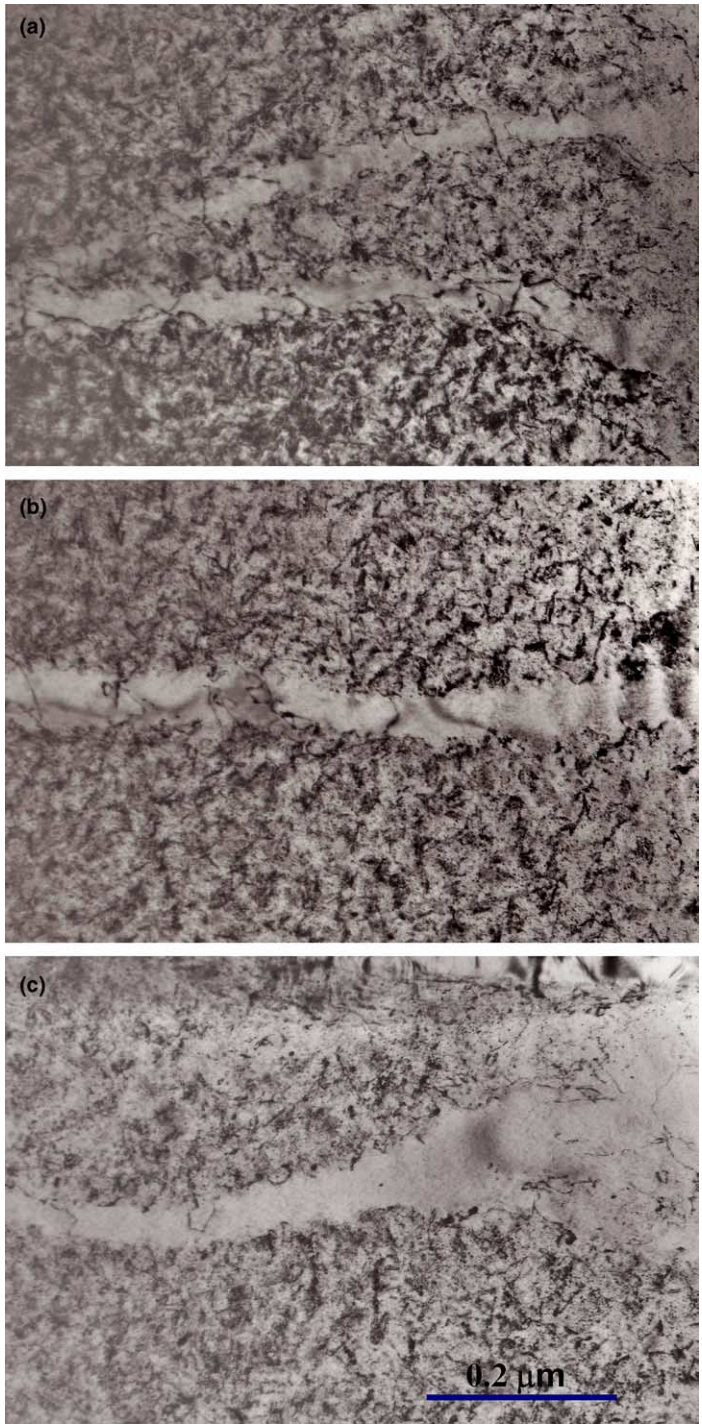


Fig. 6. Detailed morphologies of dislocation channels formed by disk bend deformation to a strain of 10% after neutron-irradiation to 0.69 dpa: (a) a bifurcation, (b) a channel with relatively constant width, and (c) a channel showing widening.

contrast to the fcc lattice where the {111} slip planes predominate, bcc crystals commonly deform by slip on {110}, {112} and {123} planes [29]. These planes have similar atom packing density and include ⟨111⟩ glide directions. Dislocation channels in an irradiated material are known to

form in the same slip systems as individual dislocation glide in the unirradiated material [1–3,6,7,11,12,40]. TEM micrographs of bcc vanadium in this study [11,12] show that channels in vanadium are formed primarily on {1 1 2} planes with a few exceptions in which channels are formed on {1 1 0} or {1 2 3} planes. No stacking fault or dissociated dislocation was observed because the stacking fault energy of vanadium is too high to dissociate dislocations. Instead, plenty of evidence for cross slip was observed in channels. An example of cross slip is given in Fig. 7; the channel formed on the (2 1 1) plane cross-slipped onto the (3 2 1) plane, or vice versa. The angle measured at the deflection of the channel is about 11°. Since the theoretically calculated angle is 10.9°, which can be calculated from the normal vectors of the two planes, the channel network seen in the figure is nearly an edge-on view. Fig. 7 also shows that four different slip planes, $(2\,1\,1)$, $(1\,2\,\bar{1})$, $(\bar{1}\,2\,\bar{3})$, and (3 2 1), have been operative to form the channel network. Considering the fact that the Burgers vector of a gliding dislocation does not change by cross slip, we can find $1/2[\bar{1}\,1\,1]$ as a common Burgers vector for the two planes. Vector calculations can also confirm that this vector is a common Burgers vector for the other two slip planes, $(1\,2\,\bar{1})$ and $(\bar{1}\,2\,\bar{3})$, and that it is parallel to the beam direction in TEM observation.

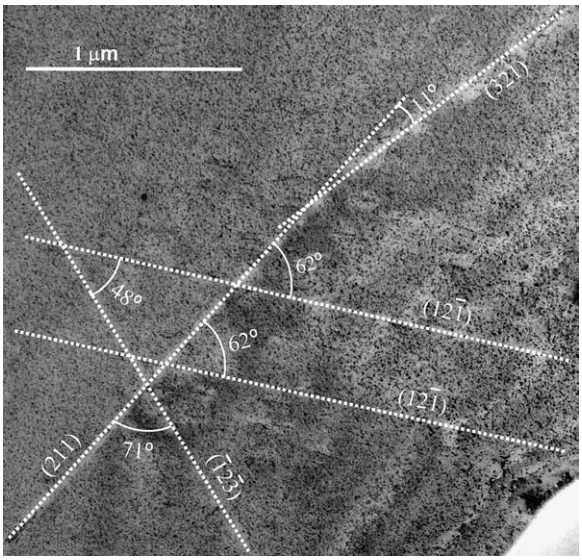


Fig. 7. A channel network with multiple channeling planes after irradiation to 0.12 dpa and deformed to a bulk plastic strain of 0.3% ($\vec{Z} \approx [\bar{1}\,1\,1]$). Cross slip occurred from the (2 1 1) plane to the (3 2 1) plane, which are at a small angle of ~11°. The angles marked were measured from the micrograph, and the channeling planes are the most probable planes. Theoretically calculated angles using the normal vectors of the planes are 10.9°, 49.1°, 60°, and 71.8°, which correspond to the measured angles 11°, 48°, 62°, and 71°, respectively. (Note that the measured and calculated angles are slightly different.) Zone axis is parallel to the Burgers vector ($\vec{Z} \approx [\bar{1}\,1\,1] \| \vec{b}$).

The curved, widening channels and frequent bifurcation of channels in Figs. 5 and 6 indicate that cross slip becomes a common process in channeling in the disk bend specimens after irradiation to a high dose. It is believed that the curved or widening channels can be formed by multiple cross slips in the curved region. Although the curved channels have been observed in some bcc metals such as molybdenum [35,41] and iron [42], channel widening has seldom been observed [34]. Since the cross slip process can occur only by screw dislocations, this widespread cross slip in channeling might indicate that most of the channeling dislocations are screw dislocations.

It is also worth mentioning that all angles measured for cross slip and widening were similar to or less than 50°. (Note that most of the micrographs showing clear channels are edge-on views.) This indicates that in vanadium the cross slip occurs between two planes with relatively small angles. Remember that in fcc materials the angle between any non-parallel {1 1 1} planes is 70.53° and no smaller angle can be formed between possible slip planes. Since localized bands such as channels and twins are formed usually at a high speed in a high stress condition, a growing channel should have momentum to advance straight. In fcc materials, therefore, it may not be easy for a fast-growing channel or twin to change its direction making such a large angle. Thus, in fcc metals cross slip might be relatively difficult to occur, even without the stacking faults that prohibit cross slip.

### 4.2. Strength of radiation-induced defect clusters

Dislocation glide and resulting deformation microstructure may be affected by the strength of radiation-induced defect clusters. However, the details of hardening mechanism by the radiation-induced defects are not fully understood [1,5]. This may be because the plastic deformation processes in irradiation-hardened materials, such as channeling and twinning, occur too rapidly to record or observe [1,6,7]. Direct observations in TEM [43] might be possible only for the materials hardened by irradiation to low doses, in which dislocation

glides are slow. For the cleared channels, few attempts have been successful for an in situ observation of initiation and propagation; modeling and computer simulation seem to be the only practical way of investigation [44,45].

Since the sizes of the obstacles in the materials irradiated at low temperatures are a few nanometers or smaller, the dispersed barrier-hardening models may be useful for predicting hardening behavior. Orowan theory [46] has been frequently applied to explain the hardening behavior of dispersion-hardened materials. However, this theory overestimates the hardening stress of irradiated materials because it assumes unremovable hard obstacles, rather than the soft defect clusters in the irradiated materials, which can be shearable or removable by gliding dislocations. To consider the effectiveness of the radiation-induced defects in the hardening process, Seeger [47] proposed a modified Orowan theory, so-called the zone theory, in which the defects are the zones that act as barriers to the gliding dislocations. Here, the expression for irradiation hardening [47–49] is adopted to measure the strength of the defect clusters in stainless steels [48,50,51] and vanadium [12,52,53] and to see if the significant difference in the strain localization features can be explained by the difference in the strength of defects. In the model the increase of yield stress by irradiation, ΔYS, is given by

$$\Delta YS = \alpha MGb\sqrt{Nd}, \tag{1}$$

where α is the strength parameter for the radiation induced defects, $M$ is the Taylor factor in polycrystalline materials, $G$ is the shear modulus, $b$ is the Burgers vector of gliding dislocations, and $N$ and $d$ are the density and diameter of the defect clusters, respectively. This equation can be used for general hardening cases, including Orowan-type hardening ($\alpha = 1$), and the term $Nd$ is assumed to be proportional to the neutron fluence in limited range [47,54].

The values of α were calculated for the irradiation cases 3 and 4 (see Tables 1 and 2) and are summarized in Table 2 along with values for parameters needed in calculation of α. Regardless of the significant differences in the strain localization behavior, both materials have similar α-values; the average values are 0.31 and 0.29 for the stainless steel and vanadium, respectively. Since this result indicates that the strengths of defects are similar for both materials, we can conclude that the strength of defects is not a significant factor in determining the shape of channels.

One of the important characteristics of channeling and twinning processes might be that the dislocations tend to glide in group in a high-stress condition [15,23]. In a highly irradiation-hardened material dislocation pileups should be formed to overcome the high critical shear stress due to the irradiation-produced obstacles. It should be noted that the aforementioned dispersion hardening models were developed by considering the interactions between multiple obstacles and a single gliding dislocation [46,47,54]. Since the stress ahead of a dislocation pileup is much higher than the stress from a single dislocation, the basis of those theories may not be valid for the current localization deformation mechanisms. In Seeger's equation [12,47–49], however, the α-parameter can be re-interpreted as a measure of the strength of defect clusters against the gliding dislocation groups. If this interpretation is correct, it can be proposed that the α-values are calculated to be well below the unity value for solid obstacles not because of the softness of the radiation induced defects but because of the effectiveness of the high stress field raised by dislocation pileups.

Table 2
Material property data and strength parameter for the radiation-induced defects (α)

| Case no. | Material | Dose (dpa) | $N$ ($m^{-3}$) | $d$ (nm) | $Nd$ | $M$ | $G$ (GPa) | $b$ (nm) | ΔYS (MPa) | α | Average α |
|---|---|---|---|---|---|---|---|---|---|---|---|
| 3 | 316SS | 0.001 | $7.4\times10^{22}$ | 1.5 | $1.11\times10^{14}$ | 3.07 | 84 | 0.252 | 101 | 0.15 | 0.31 |
| | | 0.01 | $8.1\times10^{22}$ | 0.8 | $0.65\times10^{14}$ | 3.07 | 84 | 0.252 | 233 | 0.44 | |
| | | 0.1 | $1.0\times10^{23}$ | 1.6 | $1.60\times10^{14}$ | 3.07 | 84 | 0.252 | 336 | 0.41 | |
| | | 0.78 | $4.0\times10^{23}$ | 1.8 | $7.20\times10^{14}$ | 3.07 | 84 | 0.252 | 440 | 0.25 | |
| 4 | V | 0.012 | $1.1\times10^{23}$ | 1.8 | $1.98\times10^{14}$ | 2.75 | 47 | 0.262 | 167 | 0.35 | 0.29 |
| | | 0.12 | $1.9\times10^{23}$ | 2.1 | $3.99\times10^{14}$ | 2.75 | 47 | 0.262 | 219 | 0.33 | |
| | | 0.69 | $2.3\times10^{23}$ | 2.1 | $4.83\times10^{14}$ | 2.75 | 47 | 0.262 | 144 | 0.19 | |

Yield stresses for unirradiated 316 stainless steel and vanadium are, respectively, 234 and 304 MPa. The data for $d$ and $N$ are, respectively, the mean size and total density obtained from the measured data with significant distributions.

Table 3
Stress state in sheet tensile and disk specimens [57]

| Case no. | Material | Load | Stress state | Stress triaxiality ($t = \sigma_m/\sigma_{eq}$) |
|---|---|---|---|---|
| 1 | 316LN (FCC) | Tensile | Uniaxial ($\sigma_{xx} = \sigma_{yy}$, $\sigma_{zz} = \sigma_{eq}$) | 0.33 |
| 2 | 316LN (FCC) | Disk bend | Biaxial (surface) ($\sigma_{xx} = \sigma_{yy}$, $\sigma_{zz} = 0$) | 0.67 |
| 3 | 316 (FCC) | Tensile | Uniaxial ($\sigma_{xx} = \sigma_{yy}$, $\sigma_{zz} = \sigma_{eq}$) | 0.33 |
| 4 | V (99.8% purity, BCC) | Tensile | Uniaxial ($\sigma_{xx} = \sigma_{yy}$, $\sigma_{zz} = \sigma_{eq}$) | 0.33 |
| 5 | V (99.8% purity, BCC) | Disk bend | Triaxial (middle) ($\sigma_{xx} = \sigma_{yy}$, $\sigma_{zz} < 0$) | ~0.25 |

### 4.3. Effect of stress state

In polycrystalline materials, the stress field within a crystal will always be multiaxial even under a uniaxial applied load. This is because crystal deformation is elastically and plastically anisotropic, which induces interactions between adjoining crystals. Especially in plastic deformation, dislocation, glide occurs in a limited number of slip systems in each crystal and therefore, probably almost always, the multiaxial stress field within a crystal cannot be fully relaxed by any possible combination of dislocation slips. In such a circumstance a crack or dislocation pileup (or forest) must be formed to accommodate the mismatch, which is often called the incompatibility strain [55,56]. Some forms of the incompatibility strain, such as dislocation pileups at a grain boundary, will give rise to long-range internal (or back) stress and contribute to strain hardening. Since more slip systems are available in bcc metals than in fcc or hcp metals [29], it is expected that the accumulation of incompatibility strain during plastic deformation will be lower in bcc metals, and so will be the strain hardening rate. This is generally true in the initial stage of plastic deformation.

Under a multiaxial macroscopic loading, the stress field within a grain will be more complex. In the present work complex stress fields were obtained by the ball indentation technique (see cases 2 and 5 in Table 3). The stress field in the material under a ball is an axisymmetric field with radial and axial gradients [21,57]. In such complex stress state dislocation slips must accommodate the stress field with curvature and gradients. In a crystal during plastic deformation, slip systems will operate in such a way that the stress or stored elastic energy at the grain can be minimized. Excluding the possibility of internal cracking, the operation of as many as possible slip systems and cross slips may be the most effective way to achieve the minimum energy. In the bend deformed disks, therefore, complex shapes of channels are observed as seen in Figs. 5 and 6. In a macroscopic stress state, the stress triaxiality, $t$ ($= \sigma_m/\sigma_{eq}$, where $\sigma_m$ is the mean stress of the three principal component and $\sigma_{eq}$ is the equivalent stress) for a uniaxial tensile load is 0.33, and those for indentation loading were about 0.67 and 0.25 at the bottom surface (or the opposite side of ball contact) and at the center of the disk specimen, respectively, as listed in Table 1. Any deviation from the value for uniaxial loading, 0.33, indicates a constraint higher than in the uniaxial loading. Similarly complex channels are expected in the necked region of a tensile specimen, where the stress triaxiality can be as high as that at the disk surface [57]. Unfortunately, sampling for TEM from the necked region of vanadium specimen was not possible in the present work because of the prompt necking after irradiation to doses above ~0.01 dpa and the very localized size of the necked region. The complex structure of channels is believed to be common in high strength material deformed by multiaxial loading. For example, in a compression-loaded irradiated molybdenum specimen, a complex structure of stair-rod channels, dislocation tangles, and zigzag channels were generated due to a complex stress state in the end portion of the specimen [35].

## 5. Conclusion

Microscopic strain localization in irradiated 316 and 316LN stainless steels and pure vanadium was investigated, focusing on the shape of localized deformation bands. The specimens were deformed by a uniaxial tensile load or by a multiaxial indentation load after irradiation at temperatures between 50 and 200 °C. The TEM microstructures were compared and analyzed to reveal differences between the fcc stainless steels and bcc vanadium. Key conclusions from this study are given as follows:

[1] In the 316 stainless steels, stacking faults and twins were dominant after deformation of specimens helium irradiated to 0.1 dpa or

higher, while cleared channels were dominant after neutron irradiation to a dose of 0.78 dpa. Both the uniaxial tensile loading and the multiaxial bend loading produced straight channels and twins which form well-defined narrow bands.

[2] In vanadium specimens, curved channels were observed after tensile deformation and were a common feature after multiaxial bend deformation. Further, the channel width was not constant along the channels; the widening of channels occurred during channel growth. These curved or widening channels are considered to be the evidence for successive cross slips by screw dislocations.

[3] Slip systems for the localized dislocation glide processes in irradiated specimens (channeling and twinning) are the same as in the random glide processes commonly observed in unirradiated materials.

[4] It is believed that the dissociation of dislocations into partials and the high angles between easy glide planes in the stainless steel suppress cross slip and therefore inhibits the formation of curved or widening channels. In vanadium, the multiaxial stress state increases the tendency for channel bending and widening.

## Acknowledgements

This research was sponsored by US Department of Energy, Office of Fusion Energy Sciences, under Contract DE-AC05-00OR22725 with UT-Battelle, LLC. The authors would like to express special thanks to Drs S.J. Zinkle, J.T. Busby, and R.L. Klueh for their technical reviews and thoughtful comments.

## References

[1] M.S. Wechsler, The Inhomogeneity of Plastic Deformation, American Society for Metals, Metals Park, OH, 1971 (Chapter 2).
[2] J. Gittus, Irradiation Effects in Crystalline Solids, Applied Science Publisher, London, 1978.
[3] F.A. Smidt Jr., Dislocation channeling in irradiated metals, NRL Report 7078, Naval Research Laboratory, Washington, DC 20390, June 3, 1970.
[4] R.P. Tucker, M.S. Wechsler, S.M. Ohr, J. Appl. Phys. 40 (1969) 400.
[5] M.J. Makin, J.V. Sharp, Phys. Statist. Sol. 9 (1965) 109.
[6] J.V. Sharp, Philos. Mag. 16 (1967) 77.
[7] J.V. Sharp, Acta Metal. 22 (1974) 449.
[8] A. Luft, Progr. Mater. Sci. 35 (1991) 97.
[9] T.H. Blewitt, R.R. Coltman, R.E. Jamison, J.K. Redman, J. Nucl. Mater. 2 (1960) 277.
[10] B.N. Singh, A. Horsewell, P. Toft, J. Nucl. Mater. 271&272 (1999) 97.
[11] K. Farrell, T.S. Byun, N. Hashimoto, Oak Ridge National Laboratory Report, ORNL/TM-2003/63, 2003.
[12] N. Hashimoto, T.S. Byun, K. Farrell, S.J. Zinkle, J. Nucl. Mater. 336 (2005) 225.
[13] N. Hashimoto, T.S. Byun, K. Farrell, J. Nucl. Mater. 329–333 (2004) 947.
[14] N. Hashimoto, T.S. Byun, K. Farrell, Microstructural analysis of deformation in neutron-irradiated FCC materials, J. Nucl. Mater., in press.
[15] T.S. Byun, N. Hashimoto, K. Farrell, Deformation mode map of irradiated 316 stainless steel in true stress-dose space, J. Nucl. Mater., in press.
[16] C. Bailat, A. Almazouzi, N. Baluc, R. Schaublin, F. Groschel, M. Victoria, J. Nucl. Mater. 283 (2000) 446.
[17] J.I. Cole, S.M. Bruemmer, J. Nucl. Mater. 225 (1995) 53.
[18] E.H. Lee, T.S. Byun, J.D. Hunn, M.H. Yoo, K. Farrell, L.K. Mansur, Acta Mater. 49 (2001) 3269.
[19] E.H. Lee, M.H. Yoo, T.S. Byun, J.D. Hunn, K. Farrell, L.K. Mansur, Acta Mater. 49 (2001) 3277.
[20] E.H. Lee, T.S. Byun, J.D. Hunn, K. Farrell, L.K. Mansur, J. Nucl. Mater. 296 (2001) 183.
[21] T.S. Byun, E.H. Lee, J.D. Hunn, K. Farrell, L.K. Mansur, J. Nucl. Mater. 294 (2001) 256.
[22] T.S. Byun, E.H. Lee, J.H. Hunn, J. Nucl. Mater. 321 (2003) 29.
[23] T.S. Byun, Acta Mater. 51 (2003) 3063.
[24] R.W. Hertzberg, Deformation and Fracture Mechanics of Engineering Materials, 3rd Ed., John Wiley, New York, 1989.
[25] Z. Jin, T.R. Bieler, Philos. Mag. A 72 (1995) 1201.
[26] Z. Jin, T.R. Bieler, Philos. Mag. A 71 (1995) 925.
[27] T.S. Byun, K. Farrell, Acta Mater. 52 (2004) 1597.
[28] T.S. Byun, N. Hashimoto, K. Farrell, Acta Mater. 52 (2004) 3889.
[29] M.A. Meyers, K.K. Chawla, Mechanical Behavior of Materials, Prentice-Hall, Upper Saddle River, NJ, 1998.
[30] J.P. Hirth, J. Lothe, Theory of Dislocations, McGraw-Hill, New York, 1968.
[31] S.S. Shin, M.C. Fivel, M. Verdier, K.H. Oh, Philos. Mag. 83 (2003) 3691.
[32] E.H. Lee, Nucl. Instrum. and Method. B151 (1999) 29.
[33] E.H. Lee, T.S. Byun, J.D. Hunn, N. Hashimoto, K. Farrell, L.K. Mansur, J. Nucl. Mater. 281 (2000) 65.
[34] Y. Huang, R.J. Arsenault, Rad. Eff. 17 (1973) 3.
[35] D.F. Hasson, Y. Huang, E. Pink, R.J. Arsenault, Metall. Trans. 5 (1974) 271.
[36] A.H. Cottrell, Theory of Crystal Dislocations, Gordon and Breach, New York, 1964.
[37] A. Kelly, G.W. Groves, Crystallography and Crystal Defects, J.D. Arrowsmith, London, 1970.
[38] L.E. Murr, Interfacial Phenomena in Metals and Alloys, Addision-Wesley, New York, 1975.
[39] T.S. Byun, K. Farrell, E.H. Lee, J.D. Hunn, L.K. Mansur, J. Nucl. Mater. 298 (2001) 269.
[40] H. Mughrabi, D. Ströhle, M. Wilkens, Z. Metall. 72 (5) (1981) 300.
[41] J.L. Brimhall, Trans. Met. Soc. AIME 233 (1965) 1737.

[42] S.J. Zinkle, B.N. Singh, J. Nucl. Mater. 283–287 (2000) 306.
[43] Y. Matsukawa, S.J. Zinkle, J. Nucl. Mater. 329–333 (2004) 919.
[44] Y.N. Osetsky, R.E. Stoller, Y. Matsukawa, J. Nucl. Mater. 329–333 (2004) 1228.
[45] Z. Rong, V. Mohles, D.J. Bacon, Y.N. Osetsky, Philos. Mag. 85 (2005) 171.
[46] E. Orowan, Symposium in Internal Stresses in Metals and Alloys, Institute of Metals, London, 1948, p. 451.
[47] A.K. SeegerProceedings of the 2nd International Conference on Peaceful Uses of Atomic Energy, vol. 6, IAEA, Vienna, 1958, p. 250.
[48] U.F. Kocks, Mater. Sci. Eng. 27 (1977) 291.
[49] S.J. Zinkle, Rad. Eff. Def. Solids 148 (1999) 447.
[50] S.J. Zinkle, R.L. Sindelar, J. Nucl. Mater. 196 (1988) 258.
[51] N. Hashimoto, E. Wakai, J.P. Robertson, J. Nucl. Mater. 273 (1999) 95.
[52] H. Matsui, O. Yoshinari, K. Abe, J. Nucl. Mater. 885 (1986) 114.
[53] E.R. Bradley, R.H. Jones, J. Nucl. Mater. 901 (1981) 103.
[54] B.N. Singh, A.J.E. Foreman, H. Trinkaus, J. Nucl. Mater. 249 (1997) 103.
[55] M.F. Ashby, Philos. Mag. 21 (1970) 413.
[56] M.A. Meyers, E. Ashworth, Philos. Mag. 46 (1982) 737.
[57] T.S. Byun, J.W. Kim, J.H. Hong, J. Nucl. Mater. 252 (1988) 187.